MIT Libraries | DSpace@MIT

MIT Open Access Articles

Molecular dependencies of dynamic stiffening and strengthening through high strain rate microparticle impact of polyurethane and polyurea elastomers

Massachusetts Institute of Technology

Molecular Dependencies of Dynamic Stiffening and Strengthening through High Strain Rate Microparticle Impact of Polyurethane and Polyurea Elastomers

Yuchen Sun[1,2,*], You-Chi Mason Wu[1,2], David Veysset[2], Steven E. Kooi[2], Weiguo Hu[4], Timothy M. Swager[1,2], Keith A. Nelson[1,2], Alex J. Hsieh[2,3]

[1]*Department of Chemistry, MIT, Cambridge, Massachusetts 02139, USA*
[2]*Institute for Soldier Nanotechnologies, MIT, Cambridge, Massachusetts 02139, USA*
[3]*U.S. Army Combat Capabilities Development Command, Army Research Laboratory,*
FCDD-RLW-MG, Aberdeen Proving Ground, Maryland 21005-5069, USA
[4]*University of Massachusetts, Department of Polymer Science & Engineering, Amherst, MA 01003, USA*

This study investigates the molecular dependencies of dynamic stiffening and strengthening through comparison of high strain rate impact responses of various polyurethanes and polyureas. We use an in-house designed tabletop micro-impact experimental platform—the laser-induced particle impact test (LIPIT)—to perform high strain rate impacts and measure the corresponding material response. Dynamic mechanical analysis and differential scanning calorimetry are used to show that glass transition temperature is a useful predictor of impact response at ambient temperatures. Meanwhile, solid-state nuclear magnetic resonance spectroscopy identifies segmental dynamics as an important determinant of the variation in both dynamic stiffening and strengthening. The impact responses of polyurethanes and polyureas both show clear dependencies on the molecular weight of the soft segment. This comparison suggests the state of intermolecular hydrogen bonding plays a key role in dynamic stiffening and strengthening. This study aims to identify the molecular dependencies of impact response and establish a foundation for further design and testing of optimal high strain rate characteristics in synthetic elastomers.

---

[*] Corresponding author.
E-mail address: ysun7@mit.edu (Y. Sun).

1

Segmented elastomers including polyurethanes[1–4], polyureas[5–12], and poly(urethane urea)s[13–21] are a unique class of chemically versatile materials that have been extensively investigated. These materials possess complex microstructure and span a broad range of physical and mechanical properties. Renewed interest in high-performance segmented elastomers emerged from the experimental realization of their potential for robust ballistic impact response through tailored segmental dynamics[5]. Materials that can exhibit dynamic stiffening, i.e., a shift from rubbery behavior at ambient conditions towards glassy-like behavior upon high strain rate deformation, were shown to be capable of enhanced energy absorption and dissipation[5]. Meanwhile, the influence of molecular moieties has also been reported to be increasingly important on the dynamic behavior of polymers as impulses become faster[22].

The laser-induced particle impact test (LIPIT) is an in-house designed tabletop method for micro-impact experiments.[23] The LIPIT is capable of inducing impacts with strain rates on the order of 10^6–10^8 s^{-1} and has been used for testing high strain rate impact responses in gels[24], segmented elastomers[19–21,25], and other various materials[26–28]. Using this platform, Hsieh et al. found that intersegmental mixing between the soft and hard phases strongly affected the high strain rate impact response of poly(urethane urea) and polyurea elastomers[21]. Wu et al. recently used solid-state nuclear magnetic resonance spectroscopy (ssNMR) and attenuated total reflectance–Fourier transform infrared spectroscopy (ATR–FTIR) data along with LIPIT experiments to provide a comprehensive discussion on the importance of an intersegmental hydrogen bonding network for dynamic stiffening in two-component polyurethanes without segregated hard domains[25].

Polyurethanes are ideal candidates for the systematic study of dynamic response due to their widely tunable chemical constituents. Changing particular attributes enables the precise study of various molecular dependencies of dynamic stiffening. As stated above, Wu et al. demonstrated the importance of intersegmental hydrogen bonding by studying two-component polyurethanes with differing isocyanates, either 4,4'-methylene diphenyldiisocyanate (MDI) or hexamethylenediisocyanate (HDI). We further the systematic study of dynamic stiffening with the LIPIT, focusing on synthetic three-component polyurethanes based on MDI, butanediol (BDO), and poly(tetramethylene oxide) (PTMO). The addition of the chain extender BDO in these three-component polyurethanes allows greater control over material characteristics including microstructure, hard segment content, and mechanical properties and facilitates study of the effects of chemistry on mechanical behavior. Ultimately, we aim to establish a systematic approach to the design of optimal mechanical properties through chemistry and testing of such synthetic elastomers.

PTMO, MDI, BDO, HDI, and dibutyltin dilaurate were purchased from Sigma-Aldrich and used as received. Tetrahydrofuran (THF) (J.T.Baker) was first dispensed from a solvent purification system (Innovative Technologies) containing activated alumina columns and then stored under argon over 4Å molecular sieves. A modified-MDI curative, polycarbodiimide-modified diphenylmethane diisocyanate, (Isonate 143L) was purchased from RCS Rocket Motor Components and oligomeric diamines (Versalink® P650 and P1000), based on poly(tetramethylene oxide di-*p*-aminobenzoate) with the molecular weight of PTMO, 650 and 1000 g/mol, respectively, from Evonik. Other solvents were purchased from commercial sources and used as received.

The three-component polyurethanes were synthesized using a two-step pre-polymer route. MDI and PTMO were first reacted to form MDI-capped PTMO-MDI oligomers followed by addition of BDO to complete polymerization in a solution phase synthesis to yield MDI-BDO-PTMO based

polyurethanes. Two polyurethanes were synthesized in this fashion, MDI-BDO-650 and MDI-BDO-1000, where the molecular weight of PTMO is 650 and 1000 g/mol, corresponding to shorter and longer chain length, respectively. The corresponding weight percentage (wt%) of hard segment content (%HS) was calculated using equation 1 shown below as 48% and 37%, respectively,
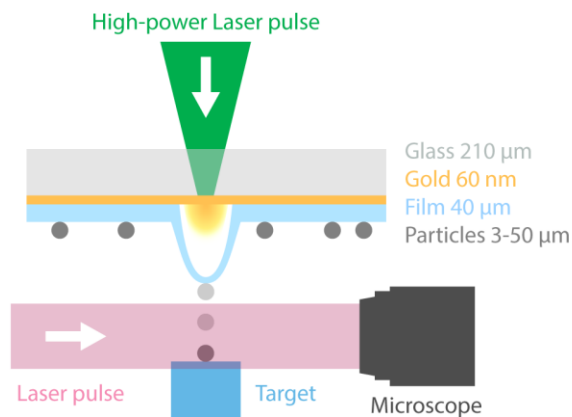
$$\%HS = \frac{(R)M_{di} + (R-1)M_{bd}}{M_g + (R)M_{di} + (R-1)M_{bd}} \qquad (1)$$

where R is the molar ratio of the diisocyanate to PTMO, and M_{di}, M_{bd}, and M_g are the number average molecular weights of MDI, BDO, and PTMO, respectively[17].

Polyureas were synthesized by mixing a modified-MDI isocyanate curative with an oligomeric diamine in a 1:1 stoichiometric ratio. This synthesis yielded two polyurea polymers, PU-650 and PU-1000, where the molecular weight of PTMO is 650 and 1000 g/mol, respectively. The weight percent of hard segment was calculated to be 50% and 33%, respectively.

Micro-impact experiments were conducted with the LIPIT. As illustrated in Fig. 1, the LIPIT uses a high-power laser pulse (Nd-YAG, 532-nm wavelength, 10-ns duration) to eject microparticles from a launching pad towards a target placed 2 cm below. The launching pad is composed of a glass substrate (210-µm thick), a sacrificial gold layer (60-nm thick), an elastomer film (polyurea, 40-µm thick), and particles distributed onto the film. The high-power laser pulse ablates the gold, expands the film, and ejects a particle at high speeds towards the target. The impact velocity is varied by tuning the energy of the high-power laser pulse. The impact event is illuminated with a second laser pulse (640-nm wavelength, 30-µs duration) and is subsequently captured through a microscope objective by an ultra-high-speed camera (SIMX16, Specialised Imaging) consisting of 16 independently triggered ICCD cameras with a minimum exposure time of 5 ns and variable interframe time.

In this experiment, silica particles with 7.38-µm diameter were accelerated to velocities between 50 and 1300 m/s. Calculation of strain rate as the ratio between strain, estimated as one for characteristic penetration of one particle diameter, and characteristic contact time, impact velocity over particle diameter, gives strain rates on the order of 10^6–10^8 s^{-1}. Figures 2(a) and 2(b) show representative image

High-power Laser pulse

Glass 210 µm
Gold 60 nm
Film 40 µm
Particles 3-50 µm

Laser pulse   Target   Microscope

Figure 1. Schematic representation of the LIPIT at the instance when a microparticle is ejected towards a target by laser ablation of a gold layer and subsequent expansion of a film layer. Particle trajectory before and after impact is visualized by a laser pulse and ultra-high-speed camera through a microscope. In this experiment, we access strain rates on the order of 10^6–10^8 s^{-1} using 7.38-µm diameter silica particles.

sequences of impacts against MDI-BDO-650 and MDI-BDO-1000, respectively. Figure 2(a) shows the impact and subsequent rebound of a silica particle against MDI-BDO-650. The trajectories are analyzed to yield impact and rebound velocities of 463 m/s and 91 m/s, respectively. The coefficient of restitution (CoR), defined as the ratio between rebound and impact velocity or equivalently the square root of the ratio between the corresponding kinetic energies, is calculated to be 0.197. Figure 2(b) shows the impact at 510 m/s with no rebound evidenced; rather, the particle remains on the surface of MDI-BDO-1000 following impact. In the case of no particle rebound, CoR is zero.
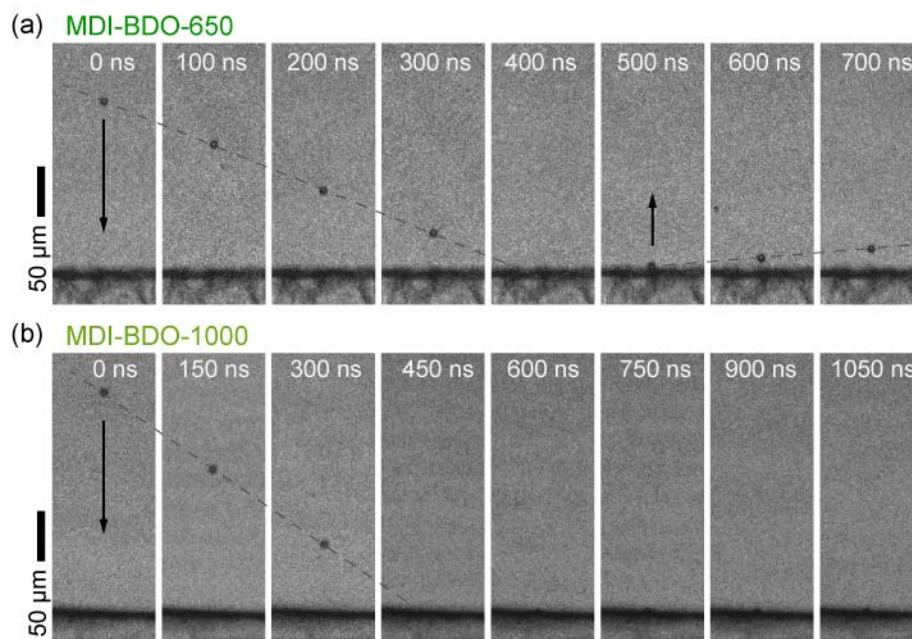
Figure 2. Representative image sequences for (a) impact of a particle on MDI-BDO-650 at 463 m/s followed by rebound and (b) impact on MDI-BDO-1000 at 510 m/s with no rebound. In both sequences, the particle initially travels downwards towards the target at the bottom of the images. Arrows denote particle direction and dashed lines illustrate particle impact and rebound speeds.

For each material, numerous impacts were performed and analyzed with curves generated to display CoR as a function of impact velocity. These CoR curves act as a comparative measure of dynamic stiffening at the strain rates associated with these high velocity impacts. Further, threshold velocity for a given material is taken as the median of the highest impact velocity inducing rebound and the lowest without rebound. Threshold velocity is reflective of dynamic stiffening and additionally dynamic strengthening and is specific to the material and the impacting particle. In this paper, we use CoR and threshold velocity as distinct and complementary measures of high strain rate impact response.

As impact velocity and strain rate approaches zero, we expect CoR to trend towards the ideally elastic limit of 1 in all materials. Figure 3 shows the CoR curves for MDI-BDO-650 and other polyurethanes[25]. Clearly at the lowest performed impacts around 50 m/s, the responses are distinctly inelastic. Notably, MDI-BDO-650 exhibits higher CoR and threshold velocity than MDI-BDO-1000, which demonstrates greater dynamic stiffening and strengthening, respectively. Meanwhile, the CoR of MDI-650 is similar to that of MDI-BDO-1000 at impact speeds up to 500 m/s, despite the two-component MDI-650 having a much lower hard segment content, 28 to 37 wt%. Moreover, MDI-650 has a remarkably higher threshold velocity than MDI-BDO-1000, suggesting a greater sensitivity in CoR
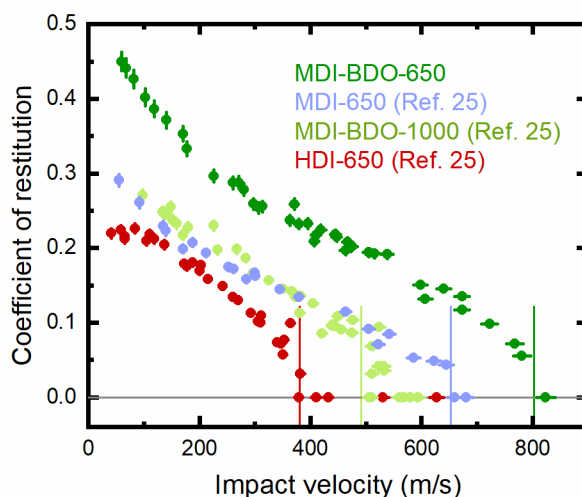
Figure 3. Comparison of coefficient of restitution (CoR) over impact velocity for polyurethanes upon impact by 7.38 µm silica spheres. Vertical lines demark threshold velocity for corresponding materials. Error bars are shown for each point. MDI-BDO-650 shows the greatest CoR and threshold velocity which corresponds to more extensive dynamic stiffening and strengthening, respectively. MDI-650 and MDI-BDO-1000 exhibit similar curves, though MDI-650 has a higher threshold velocity. Data for MDI-650, HDI-650, and MDI-BDO-1000 are reproduced from Wu et al.[25] with permission from Elsevier.

to strain rate. These high strain rate impact response measurements are the foundation on which evaluation of our synthetic elastomers are made.

Glass transition temperatures (T_g) were determined for polyurethanes with dynamic mechanical analysis (DMA) at 1 Hz and differential scanning calorimetry (DSC) at 10°C/min. The enthalpy relaxation time for DSC measurements at 10°C/min is often regarded as 100 s, corresponding to an equivalent frequency of 0.0016 Hz[6–8]. Figure 4 displays these dynamic T_g values along with the frequency range corresponding to the strain rates probed by LIPIT experiments. An increase in dynamic T_g of the materials as frequency increases from 0.0016 Hz in DSC to 1 Hz in DMA is observed. This trend is indicative of enhanced glassy-like character with increased strain rate. It is notable that the materials shown to undergo glassy transition closest and farthest from room temperature have the highest and lowest CoR, respectively. Further, based on the available data, the low frequency T_g (from DSC) of MDI-650 is closer to that of MDI-BDO-1000 while its high frequency T_g (from DMA) shifts toward MDI-BDO-650. This enhanced frequency sensitivity of T_g in MDI-650 may result from its amorphous character which promotes intermolecular hydrogen bonding between amide protons and ether carbons, opposed to the semi-crystalline HDI-650 and microphase separated three-component polyurethanes. This reflects the increased strain rate sensitivity in CoR of MDI-650 compared to MDI-BDO-1000 described previously.

Dynamic stiffening from CoR and dynamic T_g are correlated through the segmental dynamics of PTMO. Dynamic T_g reflects the segmental mobility (reciprocal of segmental dynamics) of PTMO at a given temperature. We predict dynamic stiffening to be a result of a shift from rubbery to leathery or even glassy-like behavior as strain rates approach the segmental mobility of PTMO. Additionally, this shift would impede dissociation of the intermolecular hydrogen bonds. While these materials will all

5
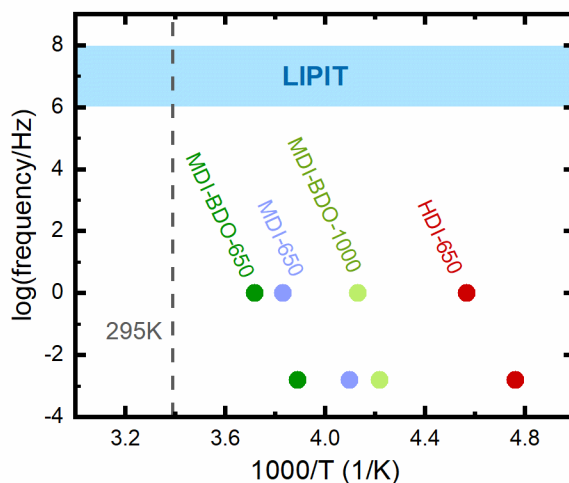
Figure 4. Comparison of the shift of T_g obtained from DMA (1 Hz) and calorimetric T_g from DSC (equivalent to 0.0016 Hz) for polyurethanes. The vertical dotted line marks room temperature and the blue zone represents strain rates associated with LIPIT impacts. Overall, T_g Notably, the T_g of MDI-650 displays greatest sensitivity to frequency, reflecting the greater sensitivity to strain rate observed in its CoR.

presumably undergo room temperature glass transition at a sufficiently high strain rate, MDI-BDO-650 is the most likely to do so at the strain rates achievable with the LIPIT. The exact strain rate required for such a transition can be determined with broadband dielectric relaxation spectroscopy.

We investigate segmental dynamics at the molecular level via ^{13}C ssNMR dipolar dephasing measurements, specifically the peak at ~71 ppm corresponding to the ether carbon of PTMO. In brief, the dipolar dephasing was determined based on the evolution of the peak area while under the influence of ^1H-^{13}C dipolar coupling. Fig. 5 compares the variation in peak area decay over time. More details into acquisition and analysis of ssNMR data is available in supplementary material. We fit the dipolar dephasing data with a two-component system, with each component representing a phase in the sample, to extract the respective decay time constants (T_{dd}) and fractions, as reported in Table S2 (see supplementary material). Phases with higher mobility are usually better represented by an exponential decay, while glassy or crystalline phases by a Gaussian curve. Fast dephasing decay corresponds to the rigid phase and slow decay to the mobile phase. Decay time constants of the mobile phase (T_{dd}^m) are listed for each polyurethane in Fig. 5, where lower T_{dd}^m indicates lower segmental mobility of mobile phase PTMO. In microphase separated elastomers such as MDI-BDO-650, the presence of phase mixing or hard segments dissolved in the soft phase increases opportunity for intermolecular hydrogen bonding. We hypothesize that increased extent of intermolecular hydrogen bonding leads to lower segmental mobility and correspondingly lower T_{dd}^m. The ordering of T_{dd}^m is consistent with that of both CoR and threshold velocity, especially for CoR where MDI-650 and MDI-BDO-1000 exhibit similar CoR and T_{dd}^m. These findings support our understanding of dynamic stiffening and strengthening as result of a shift from rubbery to leathery or even glassy-like behavior as strain rates approach the segmental mobility of PTMO.

6
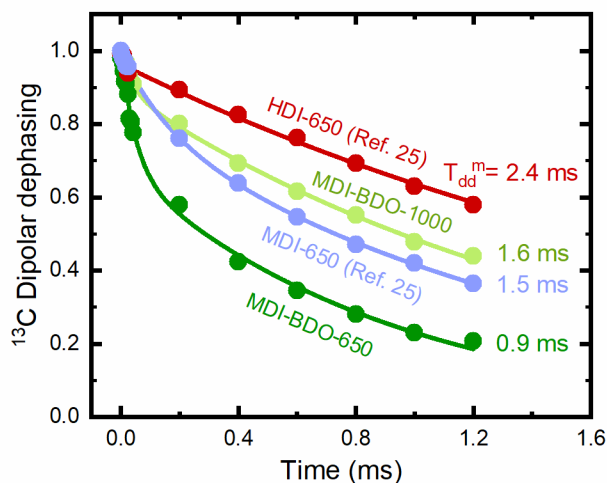
Figure 5. Comparison of ^{13}C ssNMR dipolar dephasing for polyurethanes. Lines are fits of the data to a two-phase system, mobile and rigid. Fractions and decay time constants are extracted for both phases. Decay time constants of the mobile phase (T_{dd}^{m}) are reported here. For all fractions and constants, see Table S1 (see supplementary material). Data for MDI-650 and HDI-650 are reproduced from Wu et al.[25] with permission from Elsevier.

Figure 6 displays a strong correlation between rigid-phase fraction of PTMO and threshold velocity. Notably, MDI-BDO-1000 and MDI-650 have quite different rigid-phase fractions despite having similar CoR curves. Moreover, the threshold velocities of these two materials are reflected in their rigid-phase fractions but not simply their hard segment contents. While the addition of BDO directly increases calculated hard segment content, it does not necessitate change in rigid-phase fraction of PTMO. This results from differences in crystallinity and microphase separation, revealed by comparison of HDI-650 to MDI-650 and MDI-BDO-1000 to MDI-650, respectively. Meanwhile, it is noteworthy that MDI-BDO-650 has a much higher rigid-phase fraction than MDI-BDO-1000. MDI-BDO-650 has more carbamate moieties per unit chain length and fewer ether oxygen repeat units per respective PTMO segment. This provides MDI-BDO-650 with greater propensity for intermolecular hydrogen bonding and subsequently higher rigid-phase fraction compared to MDI-BDO-1000. These data establish a connection between rigid-phase fraction associated with PTMO and dynamic strengthening through intermolecular hydrogen bonding.
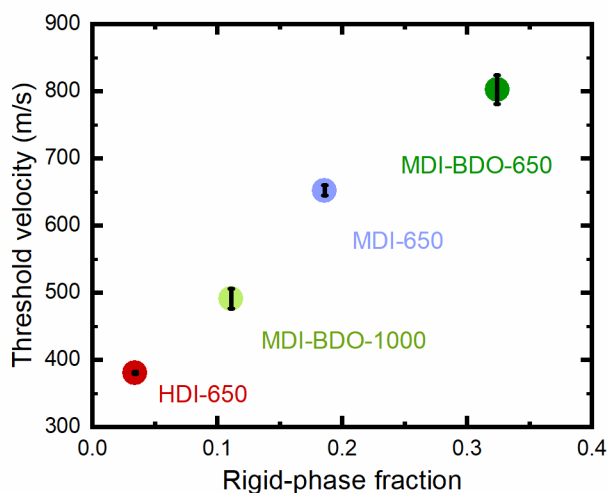
Figure 6. Comparison of threshold velocity from LIPIT to rigid-phase fraction of PTMO. Error bars for threshold velocity are shown. A strong correlation between the two values is observed, suggesting a rigid-phase fraction to play an especially important role in dynamic strengthening.

Lastly, we compare the impact response of MDI-BDO-650 with two polyureas, PU-650 and PU-1000, shown in Fig. 7. Similar to polyurethane, these polyurea materials also show that the material with a shorter soft segment length has a higher CoR and threshold velocity than its counterpart. MDI-BDO-650 and PU-1000 show remarkably similar CoR curves and nearly identical threshold velocities. It is further noteworthy that PU-650 exhibits higher CoR than MDI-BDO-650 with no observed threshold velocity at impacts up to 1300 m/s, despite the two materials having similar hard segment content. This dramatic difference in impact response likely results from differences in intersegmental hydrogen bonding between the two materials. Compared to monodentate hydrogen bonding in polyurethane, bidentate hydrogen bonding in polyurea yields stronger and more extensive hydrogen bonding interactions between the hard and soft segments, resulting in greater dynamic stiffening and dynamic strengthening.
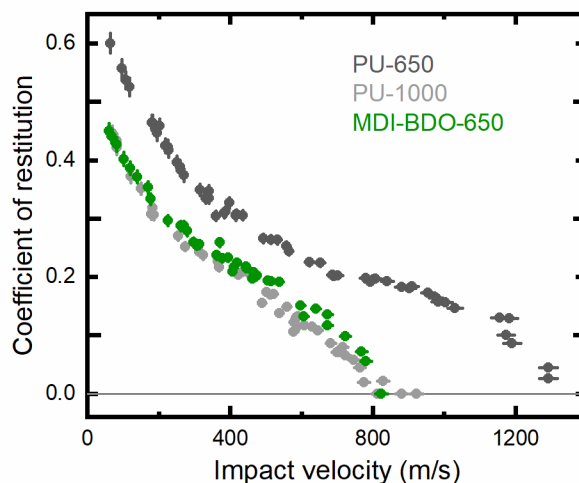
Figure 7. Comparison of coefficient of restitution over impact velocity for polyureas and MDI-BDO-650 upon impact by 7.38μm silica spheres. Error bars are shown. Although PU-650 and MDI-BDO-650 have similar hard segment contents, the polyurea exhibits higher CoR and no observed threshold velocity with impacts up to 1300 m/s. These results suggest both the strength and extent of intersegmental hydrogen bonding to play important roles in material response.

In summary, we investigated the molecular dependencies of dynamic stiffening and strengthening in polyurethanes and polyureas by comparing high strain rate impact responses from the LIPIT to measurements from DSC, DMA, and ssNMR. Results show dynamic T_g to be a useful predictor of high strain rate behaviors. We show that dynamic stiffening and dynamic strengthening depend strongly on segmental mobility of mobile-phase PTMO and that dynamic strengthening additionally depends on fraction of rigid-phase PTMO. The comparison of polyurethane and polyurea demonstrates that both soft segment length and hydrogen bonding type strongly influences impact response. The determinants of dynamic stiffening and strengthening identified in this study provide insight into the optimization of elastomeric materials. The LIPIT is used to establish a strategy for the systematic design and testing of high strain rate response in synthetic elastomers.

Acknowledgments

Supplementary Material

See supplementary material for materials characterization data obtained by DSC, as well as additional details into acquisition and analysis of phase fractions and dephasing decay time constants extracted from ^{13}C ssNMR data and calculated hard segment contents for polyurethanes.

References

[1] K. Kojio, S. Nakashima, and M. Furukawa, Polymer **48**, 997 (2007).

[2] C.B. Wang and S.L. Cooper, Macromolecules **16**, 775 (1983).

[3] J.P. Sheth, A. Aneja, G.L. Wilkes, E. Yilgor, G.E. Atilla, I. Yilgor, and F.L. Beyer, Polymer **45**, 6919 (2004).

[4] E. Yilgor, M. Isik, and I. Yilgor, Macromolecules **43**, 8588 (2010).

[5] R.B. Bogoslovov, C.M. Roland, and R.M. Gamache, Appl. Phys. Lett. **90**, (2007).

[6] C.M. Roland, D. Fragiadakis, and R.M. Gamache, Compos. Struct. **92**, 1059 (2010).

[7] D. Fragiadakis, R. Gamache, R.B. Bogoslovov, and C.M. Roland, Polymer **51**, 178 (2010).

[8] D. Fragiadakis and J. Runt, Macromolecules **46**, 4184 (2013).

[9] A.M. Castagna, D. Fragiadakis, H. Lee, T. Choi, and J. Runt, Macromolecules **44**, 7831 (2011).

[10] C.M. Roland and R. Casalini, Polymer **48**, 5747 (2007).

[11] K.E. Nugent, D.L. Ho, M.K. Vukmir, J.A. Pathak, T.H. Epps, J.N. Twigg, E.K. Lin, C.G. Robertson, P.H. Mott, and C.M. Roland, Macromolecules **41**, 7543 (2008).

[12] A.M. Castagna, A. Pangon, T. Choi, G.P. Dillon, and J. Runt, Macromolecules **45**, 8438 (2012).

[13] S.S. Sarva and A.J. Hsieh, Polymer **50**, 3007 (2009).

[14] R.G. Rinaldi, A.J. Hsieh, and M.C. Boyce, J. Polym. Sci. Part B Polym. Phys. **49**, 123 (2011).

[15] K.E. Strawhecker, A.J. Hsieh, T.L. Chantawansri, Z.I. Kalcioglu, and K.J. Van Vliet, Polymer **54**, 901 (2013).

[16] A.J. Hsieh, T.L. Chantawansri, W. Hu, K.E. Strawhecker, D.T. Casem, J.K. Eliason, K.A. Nelson, and E.M. Parsons, Polymer **55**, 1883 (2014).

[17] W. Hu, N. V. Patil, and A.J. Hsieh, Polymer **100**, 149 (2016).

[18] A.J. Hsieh, T.L. Chantawansri, W. Hu, J. Cain, and J.H. Yu, Polymer **95**, 52 (2016).

[19] D. Veysset, A.J. Hsieh, S. Kooi, A.A. Maznev, K.A. Masser, and K.A. Nelson, Sci. Rep. **6**, 1 (2016).

[20] D. Veysset, A.J. Hsieh, S.E. Kooi, and K.A. Nelson, Polymer **123**, 30 (2017).

[21] A.J. Hsieh, D. Veysset, D.F. Miranda, S.E. Kooi, J. Runt, and K.A. Nelson, Polymer **146**, 222 (2018).

[22] N.K. Bourne, J. Dyn. Behav. Mater. **2**, 33 (2016).

[23] J.-H. Lee, D. Veysset, J.P. Singer, M. Retsch, G. Saini, T. Pezeril, K.A. Nelson, and E.L. Thomas, Nat. Commun. **3**, 1164 (2012).

[24] D. Veysset, S.E. Kooi, A.A. Maznev, S. Tang, A.S. Mijailovic, Y.J. Yang, K. Geiser, K.J. Van Vliet, B.D. Olsen, K.A. Nelson, J. of the Mech. Beh. of Biomed. Mat. **86**, 71-76 (2018).

[25] Y.C.M. Wu, W. Hu, Y. Sun, D. Veysset, S.E. Kooi, K.A. Nelson, T.M. Swager, and A.J. Hsieh, Polymer **168**, 218 (2019).

[26] J. Lee, P.E. Loya, J. Lou, and E.L. Thomas, Science **346**, 1092 (2014).

[27] R. Thevamaran, O. Lawal, S. Yazdi, S.J. Jeon, J.H. Lee, and E.L. Thomas, Science **354**, 312 (2016).

[28] M. Hassani-Gangaraj, D. Veysset, K.A. Nelson, and C.A. Schuh, Scr. Mater. **145**, 9 (2018).

Supplementary materials

S1. Material characteristics

Differential scanning calorimetry (DSC) data were obtained with a TA Instruments Discovery DSC instrument, using a heat/cool/heat cycle from –90 to 180 °C at a heating/cooling rate of 10 °C/min, under a nitrogen atmosphere. The trend in T_g is as follows: MDI-BDO-650 (257K) > MDI-BDO-1000 (244K) > MDI-650 (237K) > HDI-650 (210K). Table S1 lists the T_g data obtained from DSC as well as from DMA for these polyurethanes that are shown in the dynamic T_g plot in Fig. 4.
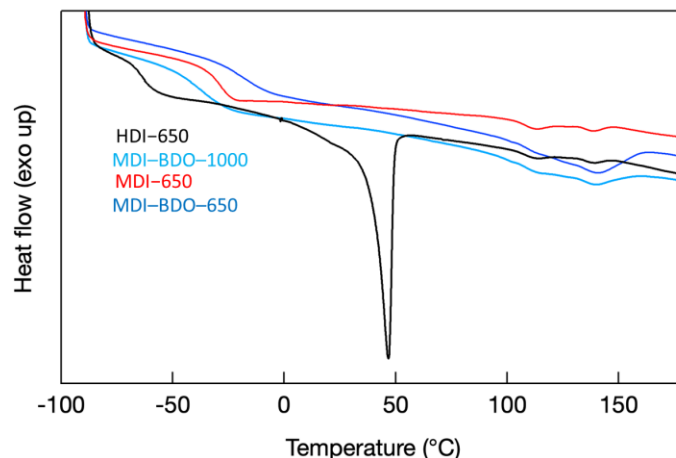
Fig. S1. DSC thermograms of HDI-650 (black), MDI-BDO-1000 (light blue), MDI-650 (red), and MDI-BDO-650 (blue).

Table S1. T_gs obtained from DSC and DMA for the tested polyurethanes.

	T_g **(K), DSC**	T_g **(K), DMA**
HDI-650	210	219
MDI-BDO-1000	237	242
MDI-650	244	261
MDI-BDO-650	257	269

.

S.2 ^{13}C ssNMR dipolar dephasing characterization

In brief, the dipolar dephasing was determined based on the evolution of the peak area at ~ 71 ppm, corresponding to the ether carbon of PTMO, under the influence of ^{1}H-^{13}C dipolar coupling. Note that these results are obtained for ether carbons of PTMO that are >= 3-4 bonds away from the carbamate groups. Meanwhile, rigid PTMO segments have strong ^{1}H-^{13}C dipolar coupling leading to faster signal decay, whereas the ^{1}H-^{13}C dipolar coupling strength of the mobile PTMO segments is attenuated by faster molecular dynamics, resulting in slower decay. The evolution times were between 1 and 42 μs, as well as multiples of rotor echo[17], which capture the fast-decaying and slow-decaying component, respectively, while minimizing the modulating effect of MAS on ^{1}H–^{13}C dipolar coupling. Additional experimental details of the ^{13}C dipolar dephasing measurements can be found in ref. 17. In

Fig. S2, representative dipolar dephasing spectra highlighting the PTMO ether carbon signal at ~ 71 ppm of MDI-PTMO-650 obtained at evolution time of 1 μs, 36 μs, and 1.2 ms are shown. Further, we fit the dipolar dephasing decay data with a two-component model with each component representing a phase in the sample. Phases with higher mobility are usually better represented by an exponential decay, while glassy or crystalline phases often well-fit with a Gaussian curve. Table S2 lists the fitting models, the phase fractions and dephasing decay time constants obtained for the respected rigid and mobile phases for polyurethanes along with corresponding hard segment content.
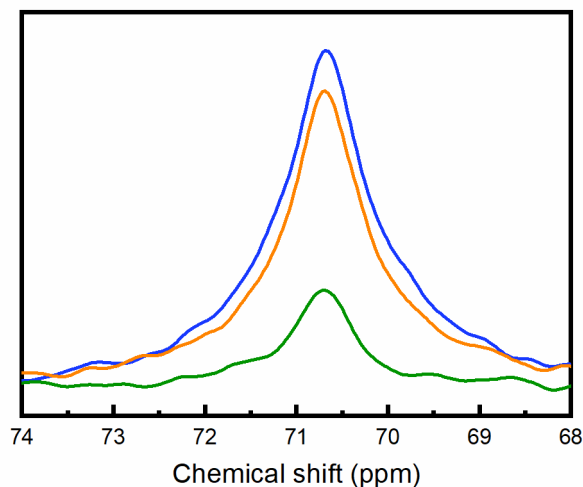
Fig. S2. Dipolar dephasing spectra of MDI-BDO-650 at evolution time of 1 μs (blue), 36 μs (orange), and 1.2 ms (green), highlighting the PTMO ether carbon signal at ~71 ppm.

Table S2. Dipolar dephasing data from ^{13}C ssNMR of polyurethanes are fitted to a two-component system using the stated fitting models. Phase fractions and dephasing decay time constants are extracted from the fits for rigid and mobile phases along with hard segment.

		Rigid phase		Mobile phase		Hard segment (wt. %)
	Fitting model	Fraction	Dephasing time (μs)	Fraction	Dephasing time (μs)	
HDI-650	Gaussian-Exponential	0.03	14	0.97	2412	21
MDI-BDO-1000	Exponential-Exponential	0.11	42	0.89	1647	37
MDI-650	Exponential-Exponential	0.19	159	0.81	1503	28
MDI-BDO-650	Exponential-Exponential	0.32	49	0.68	923	48

12